water

MDPI

Article

Experimental Analysis on the Use of Counterflow Jets as a System for the Stabilization of the Spatial Hydraulic Jump

Shokoofeh Sharoonizadeh [1], Javad Ahadiyan [1,*], Anna Rita Scorzini [2], Mario Di Bacco [2], Mohsen Sajjadi [1] and Manoochehr Fathi Moghadam [1]

[1] Department of Hydraulic Structures, College of Water Science Engineering, Shahid Chamran University of Ahvaz, Golestan Boulevard, Ahvaz 61357-43311, Iran; shsharooni@gmail.com (S.S.); m.sadjadi@scu.ac.ir (M.S.); mfathi@scu.ac.ir (M.F.M.)

[2] Department of Civil, Environmental and Architectural Engineering, University of L'Aquila, via G. Gronchi, 18-67100 L'Aquila, Italy; annarita.scorzini@univaq.it (A.R.S.); mario.dibacco@univaq.it (M.D.B.)

* Correspondence: j.ahadiyan@scu.ac.ir

Abstract: This study presents an investigation on the use of submerged counterflow jets as a means for stabilizing the spatial hydraulic jump occurring in abruptly expanding channels. The characteristics of the flow downstream from the stilling basin and the main parameters influencing the effectiveness of the device in improving flow uniformity and reducing scouring potential are examined in laboratory tests, under several geometric configurations and hydraulic boundary conditions. The position within the stilling basin and the jet density (i.e., the number of orifices issuing the counterflow jets) were found to be important parameters influencing the performance of the device. Overall, the results indicate that this dissipation system has promising capabilities in forcing the transition from supercritical to subcritical flow, by significantly shortening the protection length needed to limit the phenomena of instability associated with spatial hydraulic jumps.

Keywords: counterflow jets; energy dissipation; expanding channels; spatial hydraulic jump; stilling basin

Citation: Sharoonizadeh, S.; Ahadiyan, J.; Scorzini, A.R.; Di Bacco, M.; Sajjadi, M.; Moghadam, M.F. Experimental Analysis on the Use of Counterflow Jets as a System for the Stabilization of the Spatial Hydraulic Jump. *Water* **2021**, *13*, 2572. https://doi.org/10.3390/w13182572

Academic Editor: Chris Bradley

Received: 18 August 2021
Accepted: 13 September 2021
Published: 17 September 2021

1. Introduction

The formation of a hydraulic jump in stilling basins is frequently used as an energy dissipation system to reduce the scour downstream of hydraulic structures [1]. Methods for enhancing the energy dissipation, and thus shortening the length of the basin, have been proposed in many studies. These methods typically include the use of appurtenances, such as baffle piers, end sills, blocks, or roughness elements [2–10], while few studies also examined the possibility of using bed water jets as a means of dissipation. This last method can be a cost-effective solution, considering that water jets can be generated by deriving the flow from the upstream storage of the hydraulic structure using a system of pipes and by exploiting the head difference to the stilling basin. In particular, Tharp [11] first studied the effectiveness of injecting submerged water jets on the classical hydraulic jump. Mele and Viti [12] analyzed the effect of a secondary recirculating current caused by the difference of pressure head in two sections connected through a false floor, reporting substantial modifications in the flow patterns. France [13] used a similar arrangement to generate inclined counterflow jets in the stilling basin, describing their ability in reducing the tailwater depth required to stabilize the hydraulic jump, especially when the jet inclination generates a stronger counterflow component. These results have been recently confirmed by Alghwail et al. [14], who studied the effect of a single counterflow jet originating from a submerged orifice, by carrying out experiments with varying inclination, width, and position of the opening. They indicated optimal behavior when the jet is inclined at 45° and when it is located in the jump area, approaching the upstream section. Varol et al. [15] investigated the effect of water jets on the characteristics of hydraulic jumps, in terms of

flow structure, roller length, water surface profiles, and energy losses, while Helal et al. [16] confirmed the performance of this kind of dissipation device in improving the efficiency of submerged hydraulic jumps.

Still, practical situations exist where the downstream tailwater depth is very low and the classical jump cannot be created, even with the use of dissipation elements. In similar conditions, channel expansion can be a suitable solution [17], which, however, is prone to the possible occurrence of spatial hydraulic jumps (i.e., S-jump), characterized by unstable and asymmetric flows for specific narrow ranges of tailwater levels, for which a slight variation in the boundary condition can result in strong modifications of the cross-sectional velocity distribution and local velocity maxima [18–25]. Previous studies have demonstrated that these undesirable phenomena may be prevented or limited by inserting in the stilling basin solid sills [20,26], roughness elements [27], or cross-beam devices [24,25].

In the present study, the use of counterflow jets (i.e., opposed to the main direction of the approaching flow), generated by a transversal pipe fed by the same upstream storage supplying the main flow, is considered as an alternative dissipation system to stabilize the spatial hydraulic jump and to reduce the risk of flow asymmetry and instability phenomena in abruptly expanding channels. From a practical point of view, the device provides a double benefit, by adding the momentum of the jets to the downstream force and, at the same time, reducing the upstream flow rate, as if the return period of the flood was lower.

Several configurations, under three inflowing conditions, were first investigated to explore the system's functioning and its performance in establishing near-bed uniform flow conditions in the tailwater channel. Some of the best-performing configurations were then selected to be tested under more severe boundary conditions, providing further insights on the dissipative mechanism and on the flow field induced by the device downstream from it.

2. Materials and Methods

The experiments were carried out in a flume in the hydraulic laboratory of the Faculty of Water Science Engineering at the Shahid Chamran University of Ahvaz, Iran. The flume consisted of a storage tank (1 m wide and 2.4 m long), an ogee weir (with a height of 0.6 m and a width of 0.67 m), and a rectangular horizontal channel (12 m long, 1 m wide, and 0.87 m deep). Two plexiglass walls were installed at the toe of the weir on both sides of the channel to create a narrow section (0.6 m long and 0.67 m wide), i.e., an abrupt expansion (with an expansion ratio of b/B = 0.67 m, where b and B are, respectively, the upstream and the downstream width). A vertical sluice gate was installed in the terminal part of the flume to control the tailwater depth (Figure 1).

The first phase of the experiments was then aimed at defining these reference tailwater conditions to be used for the subsequent testing of the device. By adjusting the terminal gate, this phase then consisted of the identification of the boundary downstream water levels leading to the formation of S-jumps for the considered inflowing discharges of 56.3, 44.5, and 36.9 L/s; selected tailwater depths were equal to 0.179, 0.144, and 0.109 m for the tested Froude number Fr = 7.4, 8.7, and 9.5 ($Fr = v_1/(g \cdot h_1)^{0.5}$, where v_1 and h_1 are the velocity and the depth of the approaching flow and g is the gravitational acceleration).

Under these reference conditions, measurements of the near-bed longitudinal flow velocity were carried out with a micro-propeller (Nixon Streamflow 403–404, characterized by an accuracy of ±1.5% of true velocity) at 9 equidistant points (i.e., with a spacing of 0.1 m) on each of the 8 representative cross-sections located 0.25, 0.50, 0.75, 1.0, 1.25, 1.5, 2.5, and 8 m downstream from the abrupt expansion. The measurements were performed at a constant height of 0.5 cm from the channel bed (i.e., the minimum height achievable with the instrumentation used), for a time duration of 30 s; the time-averaged velocity was then considered for each registered time series. Water depth was also surveyed within the defined measuring grid, using a point gauge with an accuracy of ±1 mm.

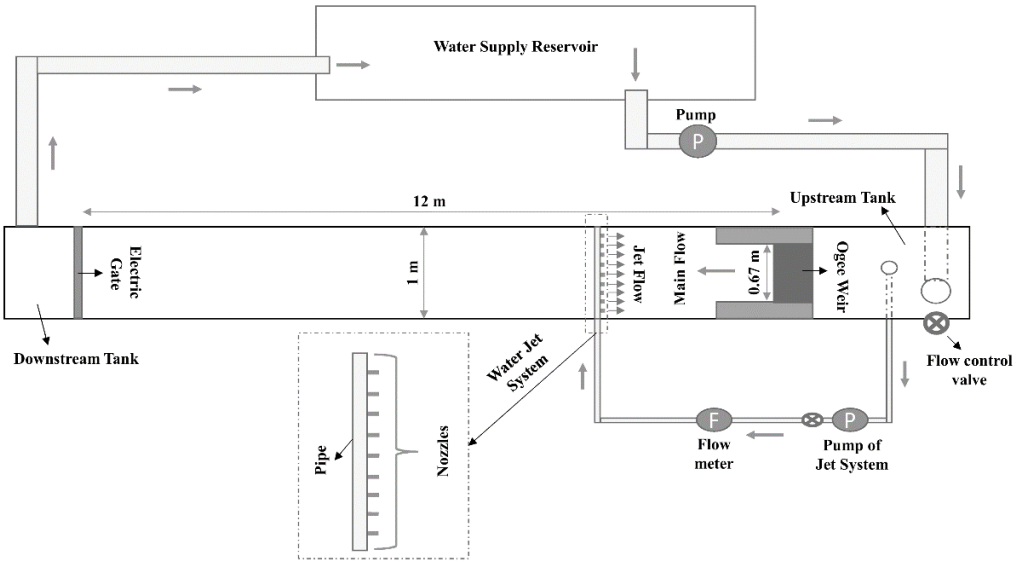

Figure 1. Schematic view of the laboratory flume.

In the second phase of the experiments, the dissipator was installed in the stilling basin. The investigated device is a water jet injection system, consisting of a 3.17 cm diameter PVC pipe orthogonally crossing the flume, with nozzles of 0.95 cm in diameter and equal spacing of 8.5 cm (Figure 2). The PVC pipe was connected to the upstream tank and the flow rate of the jets was regulated by a pump and measured with an electromagnetic flowmeter. In this experimental phase, the inlet discharge was increased compared to the one in the reference conditions, in order to keep the upstream *Fr* values constant while also supplying the jets.

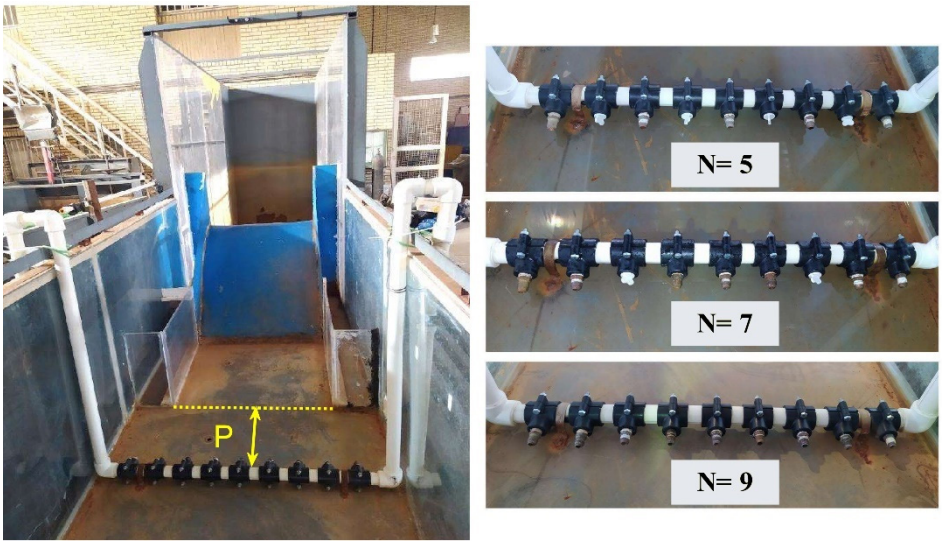

Figure 2. View of the system of counterflow jets installed in the flume, (**left**); and different tested arrangements of the jet density (i.e., varying number of open nozzles), (**right**).

A total of 54 different configurations of the device were tested, by changing the following hydraulic and geometric parameters:

- Froude number of the approaching flow (*Fr*) and the corresponding reference tailwater levels identified in the first phase (*hs*);
- Distance of the jet system from the expansion section in the flume (*P*): 0.4, 0.6, and 0.8 m;

- Jet density, i.e., number of open nozzles in water jet injection system (N): 5, 7, and 9 (Figure 2);
- Jet flow rate (Q_j): 8.1 and 7.2 L/s.

In the experimental runs with the installed device, the measurements of flow velocity and depth were executed analogously to the first phase, but only in two control sections, located 0.5 m downstream from the dissipator, and at the terminal section at 8 m from the expansion. The position of the first measurement section, which can be considered a suitable end section for the stilling basin (i.e., downstream from the region where the main dissipative phenomena take place), was identified in preliminary tests in order to ensure an unbiased comparison of the devices.

The performances of the different configurations were evaluated by comparing the near-bed flow features observed downstream from the device to the ones of the original S-jump conditions. For the characterization of the flow uniformity in quantitative terms, Scorzini et al. [24] introduced the parameter β_b, which is a modified version of the Boussinesq momentum correction coefficient for near-bed velocity:

$$\beta_b = \frac{\int_0^B v_b(x) \cdot |v_b(x)| dx}{B \cdot v_{mb}^2} \quad (1)$$

where B is the channel width, $v_b(x)$ is the near-bed longitudinal velocity across the section, and v_{mb} is the average value of $v_b(x)$.

The product $\beta_b \cdot {v_{mb}}^2$ provides information on the dynamic force of the flow (per unit height at the measurement depth) and then on its scouring potential, which is important when assessing the effectiveness of a stilling basin downstream from a hydraulic structure. β_b and $\beta_b \cdot {v_{mb}}^2$ were computed for both the reference and the 54 "with device" conditions, thus allowing for a comparative analysis of the performances of the different tested configurations of the dissipator.

In addition, a global assessment of the dissipated energy between the reservoir (E_1) and the control section at 0.5 m downstream from the device (E_2) was carried out based on the experimental measurements. In calculating the efficiency ($\Delta E = (E_1 - E_2)/E_1$), the kinetic energy correction coefficient was neglected for the upstream section (1), under the hypothesis of uniform velocity distribution, while for the downstream one (2), the near-bed coefficient α_b was used in lieu of the global Coriolis value (α), assuming it as representative of the whole cross-section. α_b was computed similarly to β_b based on the longitudinal velocities measured at the elevation of 0.5 cm from the channel bed:

$$\alpha_b = \frac{\int_0^B v_b(x)^2 \cdot |v_b(x)| dx}{B \cdot v_{mb}^3} \quad (2)$$

Based on the results of this analysis, three of the best-performing geometries were selected to be tested under more severe tailwater levels (75, 80, and 90% of hs) in order to investigate the effectiveness of the counterflow jets under a large spectrum of boundary conditions, as may occur in the actual operating conditions of a hydraulic structure. In this phase, 3D velocity measurements (with an electromagnetic velocity meter (JFE Advantech Co. ACM3-RS 3 axis, with an accuracy of ±2% of true velocity)) in four different cross-sections, located 0.25, 0.5, 1, and 2 m downstream from the dissipator, allowed a more detailed reconstruction of the flow velocity field in the tailwater channel, with the possibility of calculating the global Coriolis and Boussinesq correction coefficients of the flow, α and β [1,28]:

$$\alpha = \frac{\int_0^A v(x,z)^2 \cdot |v(x,z)| dA}{v_m^3 \cdot A} \quad (3)$$

$$\beta = \frac{\int_0^A v(x,z) \cdot |v(x,z)| dA}{v_m^2 \cdot A} \quad (4)$$

where A is the total cross-sectional flow area, $v(x,z)$ is the longitudinal velocity over the whole cross-sectional profile, and v_m is the mean flow velocity.

This analysis also allowed the verification of the representativeness of the bed coefficients, α_b and β_b, for describing the uniformity of the flow features instead of using the global coefficients, α and β. Indeed, although both the parameters (α and α_b; β and β_b) are flow uniformity coefficients, the ones denoted with lowercase "b" consider only the velocity field in the proximity of the channel bed instead of that for the whole cross-sectional area.

Moreover, in order to obtain more information on the dissipative mechanism in the stilling basin equipped with the bed counterflow jets, for the selected configurations, pressure transducers (Hoggler Hot Series), measuring the dynamic pressure at the basin floor, were installed in the centerline of the flume at four points, located both downstream and upstream from the jets (0.25 and 0.75 m in the first case, and 0.25 and 0.85 m in the second case). For each pressure tap, data were sampled at a frequency of 200 Hz over a time duration of 60 s. Due to the turbulent flow characteristics developing within the basin, the pressure regime can be analyzed as a stochastic phenomenon. Therefore, as proposed by Toso and Bowers [29], pressure fluctuations were treated as random variables, which can be characterized by statistical parameters, such as mean, standard deviation, skewness, and kurtosis. In particular, the pressure coefficient $C_p{}'$ [29], which compares the standard deviation of the pressure head σ with the inflow velocity head, was calculated from the experimental measurements:

$$C_p{}' = \frac{\sigma}{v_1^2/2g} \tag{5}$$

where v_1 is the approaching flow velocity and g is the gravitational acceleration.

Analogous coefficients for the mean pressure head P_m and both negative and positive fluctuations from the mean, ΔP^+ and ΔP^-, were expressed as well [29]:

$$C_p = \frac{P_m}{v_1^2/2g} \tag{6}$$

$$C_{p+} = \frac{\Delta P^+}{v_1^2/2g} \quad \text{and} \quad C_{p-} = \frac{\Delta P^-}{v_1^2/2g} \tag{7}$$

3. Results and Discussion

The reproduced reference conditions are the ones typical of the spatial hydraulic jump, with the main flow concentrated at one side of the cross-section, high local velocities extending over the whole tailwater channel, and a reverse flow area on the opposite side. For all the tested hydraulic conditions, the flow reached the end of the channel without completing the transition to subcritical flow. This is clearly visible in Figure 3, where β_b values are considerably greater than unity in all the measurement sections, reaching the maximum values at 2.5 m downstream from the expansion section, and still being over 2 at the end of the flume. The comparison of β_b and $\beta_b \cdot v_{mb}{}^2$ obtained with the installed device to the ones shown in Figure 3 then provides direct information on the effectiveness of the counterflow jets in stabilizing the hydraulic jump occurring in the expanding channel.

Figure 4 shows the flow patterns in the stilling basin equipped with the jet injection system. The interaction between the supercritical flow issuing from the narrow section and the counterflow jets results in a high-turbulence zone in the middle of the expansion section, with a higher flow depth and strong air entrainment, pushing away the top part of the flow and leading to local radial vortices, somewhat similar to many classical hydraulic jumps. The turbulence is almost entirely concentrated in the area upstream from the jets, resulting in quite regular subcritical flow conditions within a short distance downstream from the device, i.e., allowing for stilling basins of limited length.

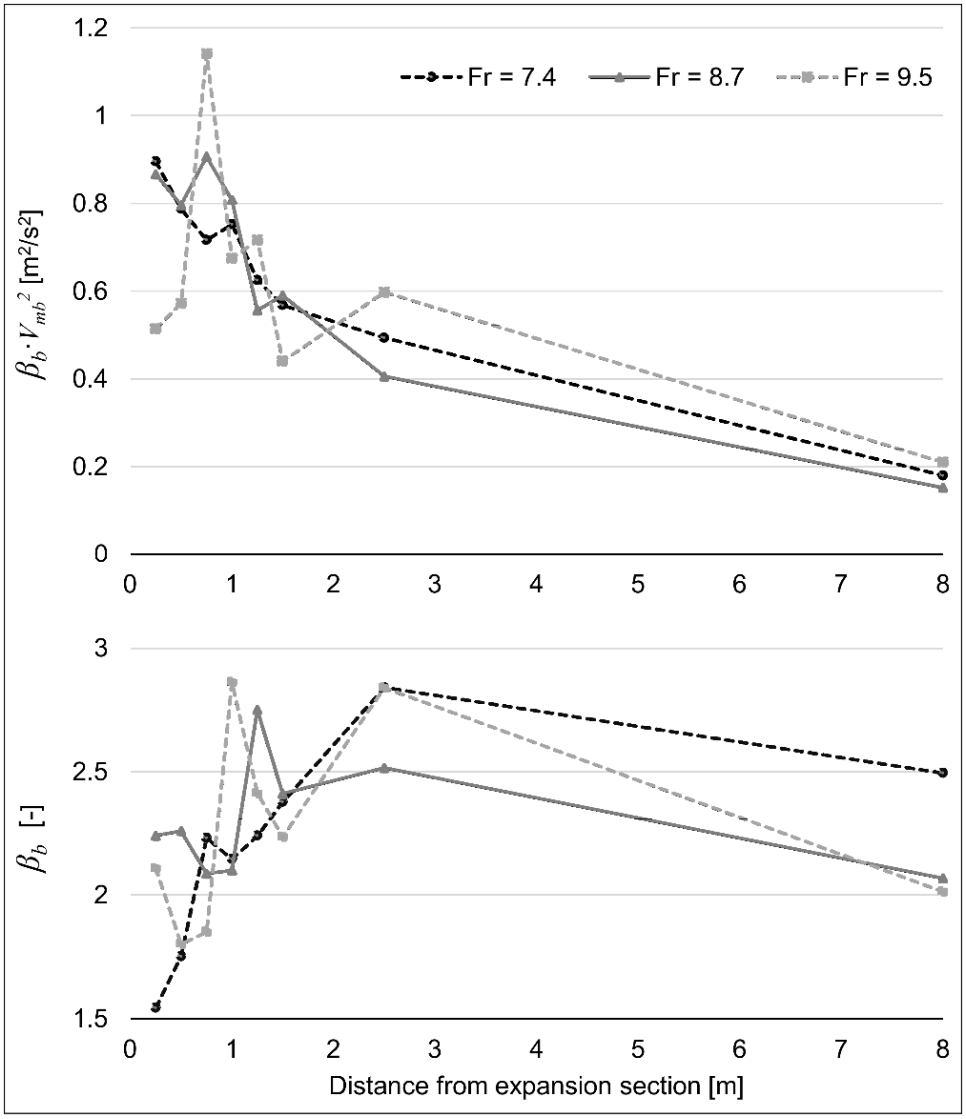

Figure 3. Values of β_b and $\beta_b \cdot v_{mb}^2$ in the measurement sections along the flume for the reference S-jump conditions.

This qualitative evidence is highlighted in quantitative terms in Figure 5, which summarizes the values of β_b and $\beta_b \cdot v_{mb}^2$ registered for all the experimental runs at the measurement section located 0.5 m downstream from the dissipator (i.e., 0.9, 1.1, and 1.3 m from the abrupt expansion for P equal to 0.4, 0.6, and 0.8 m, respectively). In this section, the flow depth was always slightly higher than the one at the end of the flume (as expected in a horizontal channel in subcritical condition) and the results for β_b (ranging from 1.01 to 1.46, with a mean of 1.15) and $\beta_b \cdot v_{mb}^2$ (the maximum registered value was equal to 0.35 m^2/s^2) reveal a good effectiveness of the system in improving the flow features in the tailwater channel, allowing the transition to subcritical flow in a stilling basin of limited length, even for the worst-performing configurations. At the end of the flume (i.e., at the measurement section at 8 m from the expansion), the flow was found to be always uniform, with β_b values constantly smaller than 1.03.

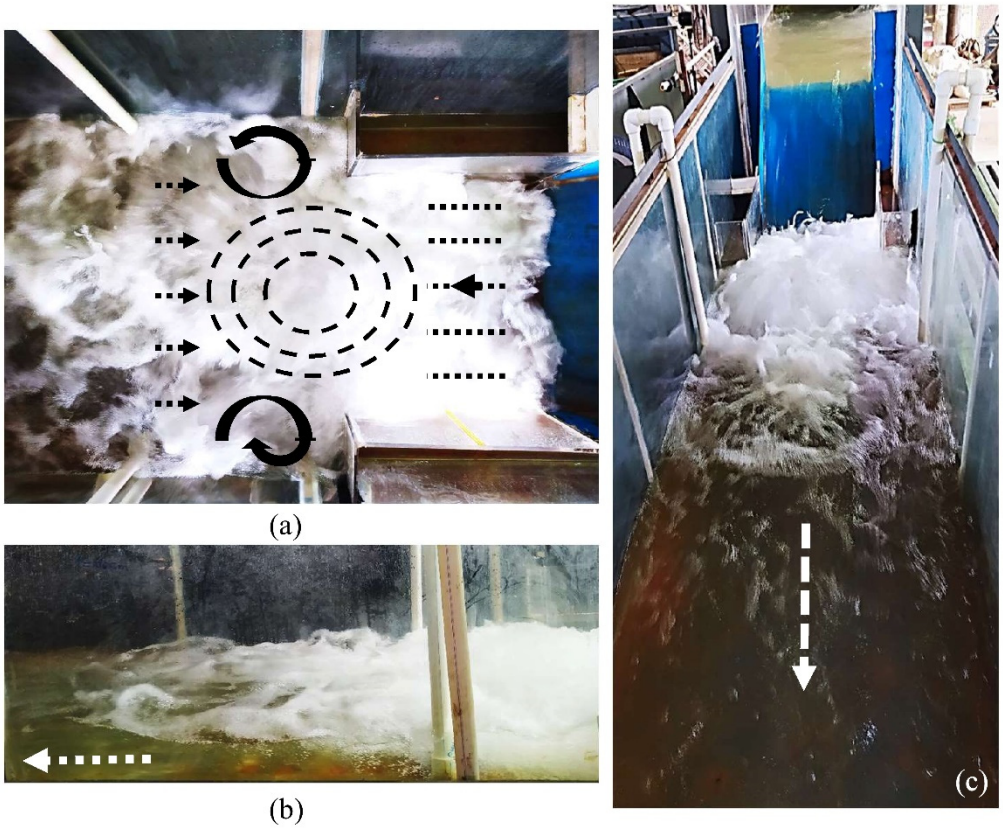

Figure 4. Typical flow patterns induced by the counterflow jets: (**a**) plan view, (**b**) side view, and (**c**) frontal view.

It should be noted that these runs were carried out under the same water levels defined in the reference conditions (*hs*), resulting in a higher downstream *Fr*, with reduced jump stabilization capability in the applications with flow-dependent boundary conditions. In addition, Figure 5 indicates that the distance of the device from the expansion section (*P*) is an influencing factor for the performance of the system, as demonstrated by the slightly higher values of β_b and $\beta_b \cdot v_{mb}{}^2$ found in the tests with the larger values of *P*.

An explanation for this behavior can be deduced from the observation of Figure S1 (in the Supplemental Materials), which shows the flow patterns in the stilling basin for two configurations of the device that differ only in the value of *P* (0.4 versus 0.8 m). It can be seen that, in the first case, the high-pressure region invades a larger portion of the narrow channel and the main flow approaches the jets with a higher velocity. Since the variation of the kinetic energy flux associated with the collision of the jets is a function of the cube of the velocity [30], this mechanism implies a higher rate of conversion into pressure head and/or energy dissipation for a given discharge, which could then explain the slightly worse performances of the devices with $P = 0.8$ m. Figure 5 also shows that the bed velocity v_{mb} has been found to increase with the jet density (i.e., higher number of open nozzles, *N*), suggesting that the flow tends to be diverted towards the free surface when the jets are less uniformly distributed across the channel. This phenomenon could be a consequence of the increase in total momentum and kinetic energy per unit of Q_j associated with a smaller number of nozzles (i.e., higher velocity of the jets), resulting in a higher local pressure upstream of the device. Regarding the influence of the jet discharge Q_j, this was found to negatively affect β_b, except for $Fr = 7.4$, while the values of $\beta_b \cdot v_{mb}{}^2$ were not surprisingly higher for increasing Q_j, because of the larger flow rate under the same downstream boundary condition.

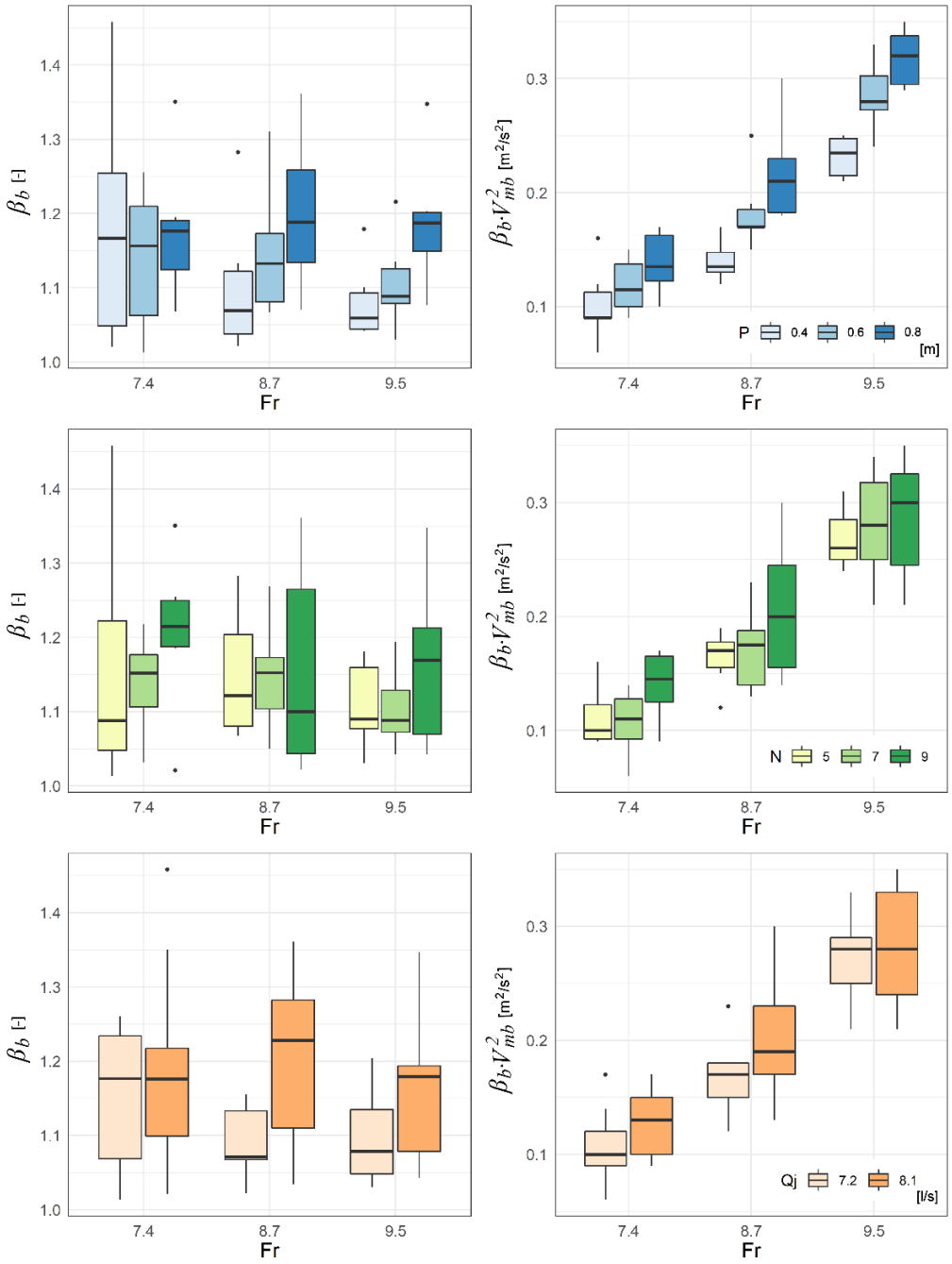

Figure 5. Performance of the dissipator as a function of *P*, *N*, and *Qj*, for the different tested *Fr*:β_b and $\beta_b \cdot v_{mb}{}^2$ registered 0.5 m downstream from the dissipator's end.

Moreover, as expected under controlled tailwater conditions, the energy dissipation was basically a function of *Fr*, with almost no influence from the geometric parameters of the device, registering a reduction in the flow energy (ΔE) of about 74, 79, and 82% for *Fr* equal to 7.4, 8.7, and 9.5, respectively.

In the second phase of the analysis, some of the most effective configurations were selected for a detailed investigation aimed at testing their performance under more severe tailwater conditions and better describing the flow features in the tailwater channel. Given the small variability observed in the behavior of the tested geometries, hereinafter, we report for illustrative purposes the results related to the following configurations (*Fr* = 7.4 in all runs):

1. Q_j = 7.2 L/s, N = 7, P = 0.4 m;
2. Q_j = 8.1 L/s, N = 9, P = 0.4 m;
3. Q_j = 7.2 L/s, N = 5, P = 0.6 m.

Figure 6 and Figures S2 and S3 (in the Supplemental Materials) provide a representation of the 3D velocity field measured downstream from the device under variable tailwater conditions, while Figure 7 summarizes the corresponding α and β values computed in the four measurement sections located downstream from the jets.

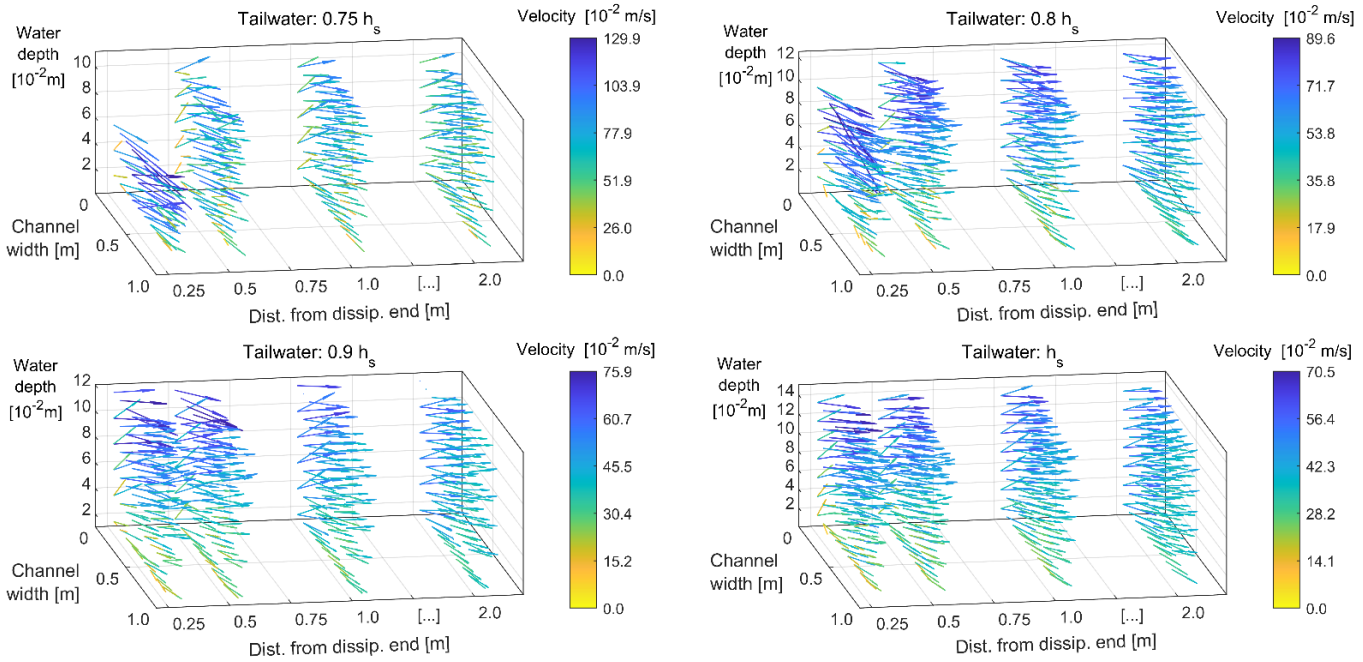

Figure 6. 3D velocity flow fields measured in the channel downstream from the dissipator, under variable tailwater conditions (as a portion of *hs*): Configuration 1 (Qj = 7.2 L/s, N = 7, P = 0.4 cm).

As expected, the flow becomes gradually more uniform when moving towards the downstream part of the flume. Higher values of α and β were registered in the first measurement section under the lowest tailwater condition (0.75 *hs*), as a consequence of a local non-stationary phenomenon characterized by a plunging effect and local oscillating water depth immediately downstream from the device, associated with pronounced air entrainment near the free surface. Except for this anomaly, the performance of Configuration 2 was found to be particularly stable also for lower tailwater levels, showing the ability of the system in stabilizing the hydraulic jump, even with lower force available downstream.

With lower tailwater conditions, the percentage of the energy dissipated in the stilling basin was increased, allowing for better exploration of the stabilization capabilities of the device. The maximum increase was registered for Configurations 1 and 2, changing from 74% under *hs* to about 79% under 0.75 *hs*. Additionally, since in this last phase of the experiments the velocity measurements were available for four whole cross-sections on a regular grid, it was also possible to evaluate the error induced by assuming $\alpha_b = \alpha$ or neglecting it in the computation of the dissipated energy, observing that the use of α_b instead of α causes an average error of 0.15%, with a maximum value of 1.16%, while neglecting it (i.e., α = 1) leads to an average error of 0.38%, thus confirming the suitability of approximating α with α_b. Moreover, in these experiments, the values of α and β were found to be linearly dependent, according to the equation $\alpha = 3.01\beta - 2.01$ (R^2 = 0.9975), in line with the observations of Mohanty et al. [31].

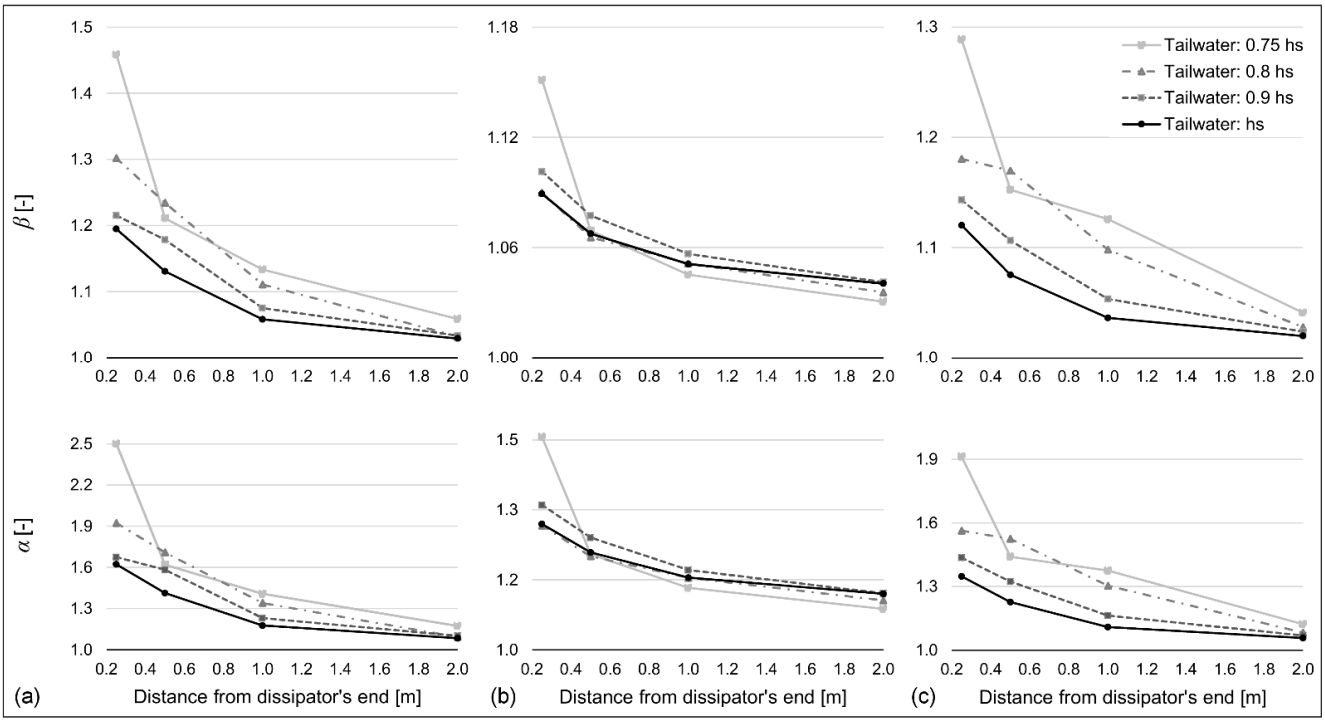

Figure 7. Momentum and kinetic energy correction coefficients (β and α) calculated downstream from the dissipator, under variable tailwater conditions: Configuration 1—Qj = 7.2 L/s, N = 7, P = 0.4 cm (**a**); Configuration 2—Qj = 8.1 L/s, N = 9, P = 0.4 cm (**b**); Configuration 3—Qj = 7.2 L/s, N = 5, P = 0.6 cm (**c**).

Finally, Figure 8 shows the calculated dimensionless bed pressure coefficients, measuring the standard deviation, mean, and maximum positive and negative deviations from the mean (Equations (5)–(7)) of the pressure fluctuations along the centerline of the flume, under Fr = 7.4 and different tailwater levels, as a function of y/P, y being the distance of each pressure transducer from the position of the counterflow jets (y/P = 1 indicates the position of the device, while y/P = 0 the expansion section).

Figure 8 refers to Configuration 1, but very similar trends have also been observed for the other two configurations considered, which are not reported here for the sake of conciseness. The panel for the mean pressure C_p roughly resembles the water surface profile, while the other plots in Figure 8 corroborate the qualitative description of the flow features provided in Figure 4.

Indeed, Figure 8 shows a reduction of the pressure fluctuations in the downstream part of the tailwater channel for all the tested tailwater depths, indicating that most of the turbulence occurs within the basin, also with maximum positive and negative pressure deviations, reaching $C_p^{\pm}$ values of about 0.5 in the expansion area. C_p' was found to increase when moving from hs to 0.75 hs, because of the additional turbulent structures induced by the jets.

However, it can be observed that minimum values attained for C_p' at y/P = 2.87 (C_p' ~ 0.1) were a bit larger than those reported in the literature for hydraulic jumps [29,32,33], suggesting that, in spite of the quite uniform flow velocity field registered (Figure 7), bed pressure oscillations are not completely contained within the basin, mainly as a consequence of the reported water surface fluctuations in the area downstream from the device [34].

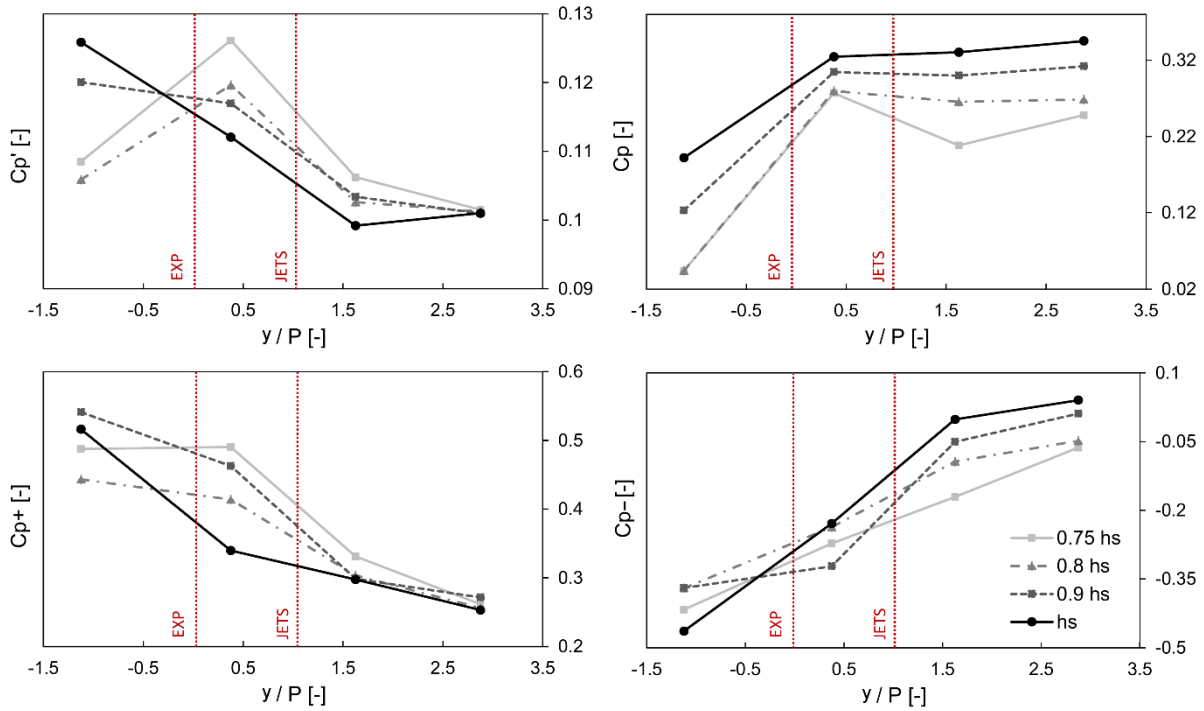

Figure 8. Bed pressure coefficients along the flume for varying tailwater levels (Configuration 1—Fr = 7.4): standard deviation of pressure fluctuations Cp', mean pressures Cp, and extreme positive and negative pressure deviations from the mean, $Cp+$ and $Cp-$.

4. Conclusions

The present study has introduced a novel dissipator, based on the use of counterflow jets, able to significantly reduce the risk of flow asymmetry and instability phenomena associated with the occurrence of spatial hydraulic jumps in abruptly expanding channels. The dissipative mechanism relies on the interaction between the incoming channel flow and the water jets issuing from the device, which breaks the main flow, causing turbulence and redistributing the velocity field in the stilling basin, with an increase of the effective water depth in the pool and the creation of recirculation zones.

In this study, 54 different configurations of the device were tested in an experimental analysis to evaluate the performance of the system in improving the flow uniformity and reducing the bed velocity in the tailwater channel. The results have shown that the distance from the expansion section and the jet density are influencing factors for its effectiveness. In the second phase, some of the best-performing configurations were selected to also test the ability of the dissipator under varying tailwater conditions and to better describe the flow patterns in the tailwater channel.

Overall, the presented experimental investigation demonstrates the promising capabilities of this device to force hydraulic jumps and control flow uniformity under a wide range of operating conditions by exploiting the collision between the jets and the incoming water, which generates a high-turbulence zone in the middle of the expansion section, with local radial vortices and strong air entrainment, particularly effective when the jets are installed near the expansion section.

Supplementary Materials: Supplementary can be found at https://www.mdpi.com/article/10.3390/w13182572/s1.

Author Contributions: Conceptualization, S.S., J.A. and M.S.; methodology, S.S., J.A., A.R.S. and M.D.B.; experimental measurements and data curation, S.S.; formal analysis, A.R.S. and M.D.B.; investigation, A.R.S. and M.D.B.; resources, M.F.M.; writing—original draft preparation, S.S. and A.R.S.; writing—review and editing, A.R.S. and M.D.B.; visualization, A.R.S.; supervision, J.A., M.S. and M.F.M. All authors have read and agreed to the published version of the manuscript.

Funding: This work was supported by the Research Council of the Shahid Chamran University of Ahvaz [grant number: 1399].

Institutional Review Board Statement: Not applicable.

Informed Consent Statement: Not applicable.

Data Availability Statement: Experimental data that support the findings of this study are available from the corresponding author upon request.

Conflicts of Interest: The authors declare no conflict of interest. The funders had no role in the design of the study; in the collection, analyses, or interpretation of data; in the writing of the manuscript, or in the decision to publish the results.

References

1. Chow, V. *Open-Channel Hydraulics*; McGraw-Hill: New York, NY, USA, 1959.
2. Rajaratnam, N. *Hydraulic Jumps. Advances in Hydroscience*; Chow, V.T., Ed.; Elsevier: Amsterdam, The Netherlands, 1967; Volume 4, pp. 197–280. ISBN 9781483199351.
3. Basco, D.R.; Adams, J.R. Drag forces on baffle blocks in hydraulic jumps. *J. Hydraul. Div.* **1971**, *97*, 2023–2035. [CrossRef]
4. Rajaratnam, N.; Murahari, V. A contribution to forced hydraulic jumps. *J. Hydraul. Res.* **1971**, *9*, 217–240. [CrossRef]
5. Peterka, A.J. *Hydraulic Design of Stilling Basins and Energy Dissipators*; United States Department of the Interior, Bureau of Reclamation: Washington, DC, USA, 1974.
6. Ohtsu, I.; Yasuda, Y.; Yamanaka, Y. Drag on vertical sill of forced jump. *J. Hydraul. Res.* **1991**, *29*, 29–47. [CrossRef]
7. Thompson, P.L.; Kilgore, R.T. *Hydraulic Design of Energy Dissipators for Culverts and Channels: Hydraulic Engineering Circular Number 14 (No. FHWA-NHI-06-086)*; National Highway Institute (US): San Diego, CA, USA, 2006.
8. Habibzadeh, A.; Loewen, M.R.; Rajaratnam, N. Performance of baffle blocks in submerged hydraulic jumps. *J. Hydraul. Eng.* **2012**, *138*, 902–908. [CrossRef]
9. Abdelhaleem, F.S.F. Effect of semi-circular baffle blocks on local scour downstream clear-overfall weirs. *Ain Shams Eng. J.* **2013**, *4*, 675–684. [CrossRef]
10. Hager, W.H. *Energy Dissipators and Hydraulic Jump*; Springer: Dordrecht, The Netherlands, 2013; Volume 8, ISBN 978-0-7923-1508-7.
11. Tharp, E.L. Modification of the Hydraulic Jump by Submerged Jets. Master's Thesis, University of Missouri, Rolla, MO, USA, 1966.
12. Mele, P.; Viti, M. Ressaut hydraulique avec recirculation. *La Houille Blanche* **1977**, *4*, 321–324. (In French) [CrossRef]
13. France, P.W. An investigation of a jet-assisted hydraulic jump. *J. Hydraul. Res.* **1981**, *19*, 325–333. [CrossRef]
14. Alghwail, A.D.A.; Stević, S.; Abourohiem, M.A. Dissipation of mechanical energy over spillway through counter flow. *Građevinar* **2018**, *70*, 377–391. [CrossRef]
15. Varol, F.; Cevik, E.; Yuksel, Y. The effect of water jet on the hydraulic jump. In Proceedings of the Thirteenth International Water Technology Conference, IWTC, Hurghada, Egypt, 12–15 March 2009; Volume 13, pp. 895–910.
16. Helal, E.; Abdelhaleem, F.S.; Elshenawy, W.A. Numerical Assessment of the Performance of Bed Water Jets in Submerged Hydraulic Jumps. *J. Irrig. Drain Eng.* **2020**, *146*, 04020014. [CrossRef]
17. Herbrand, K. The spatial hydraulic jump. *J. Hydraul. Res.* **1973**, *11*, 205–218. [CrossRef]
18. Noseda, G. An instability phenomenon of hydraulic jump in enlarging supercritical flow. *L'Energia Elettrica* **1964**, *41*, 249–254. (In Italian)
19. Rajaratnam, N.; Subramanya, K. Hydraulic jumps below abrupt symmetrical expansions. *J. Hydraul. Div.* **1968**, *94*, 481–503. [CrossRef]
20. Bremen, R.; Hager, W.H. Expanding stilling basin. *Proc. Inst. Civ. Eng. -Water Marit. Energy* **1994**, *106*, 215–228. [CrossRef]
21. Ohtsu, I.; Yasuda, Y.; Ishikawa, M. Submerged hydraulic jumps below abrupt expansions. *J. Hydraul. Eng.* **1999**, *125*, 492–499. [CrossRef]
22. Graber, S.D. Asymmetric flow in symmetric supercritical expansions. *J. Hydraul. Eng.* **2006**, *132*, 207–213. [CrossRef]
23. Zare, H.K.; Baddour, R.E. Three-dimensional study of spatial submerged hydraulic jump. *Can. J. Civ. Eng.* **2007**, *34*, 1140–1148. [CrossRef]
24. Scorzini, A.R.; Di Bacco, M.; Leopardi, M. Experimental investigation on a system of crossbeams as energy dissipator in abruptly expanding channels. *J. Hydraul. Eng.* **2016**, *142*, 06015018. [CrossRef]
25. Hajialigol, S.; Ahadiyan, J.; Sajjadi, M.; Scorzini, A.R.; Di Bacco, M.; Shafai Bejestan, M. Cross-beams dissipators in abruptly expanding channels: Experimental analysis of the flow patterns. *J. Irrig. Drain. Eng.* **2021**, *147*, 06021012. [CrossRef]
26. Zare, H.K.; Doering, J.C. Forced hydraulic jumps below abrupt expansions. *J. Hydraul. Eng.* **2011**, *137*, 825–835. [CrossRef]
27. Hassanpour, N.; Hosseinzadeh Dalir, A.; Farsadizadeh, D.; Gualtieri, C. An experimental study of hydraulic jump in a gradually expanding rectangular stilling basin with roughened bed. *Water* **2017**, *9*, 945. [CrossRef]
28. Hamidifar, H.; Omid, M.H.; Keshavarzi, A. Kinetic energy and momentum correction coefficients in straight compound channels with vegetated floodplain. *J. Hydrol.* **2016**, *537*, 10–17. [CrossRef]
29. Toso, J.W.; Bowers, C.E. Extreme pressures in hydraulic-jump stilling basins. *J. Hydraul. Eng.* **1988**, *114*, 829–843. [CrossRef]

30. Kinelovskii, S.A. Concept of elastic-inelastic interactions of jet flows and collision of jets of an ideal incompressible liquid. *Combust. Explos. Shock Waves* **1994**, *30*, 31–339. [CrossRef]
31. Mohanty, P.K.; Dash, S.S.; Khatua, K.K.; Patra, K.C. Energy and momentum coefficients for wide compound channels. *WIT Trans. Ecol. Environ.* **2012**, *172*, 87. [CrossRef]
32. Fecarotta, O.; Carravetta, A.; Del Giudice, G.; Padulano, R.; Brasca, A.; Pontillo, M. Experimental results on the physical model of an USBR type II stilling basin. In *Proceedings of River Flow 2016*; Constantinescu, G., Garcia, M.H., Hanes, D.M., Eds.; Taylor & Francis Group: London, UK, 2016; pp. 242–248. ISBN 978-1-138-02913-2.
33. Hassanpour, N.; Hosseinzadeh Dalir, A.; Bayon, A.; Abdollahpour, M. Pressure Fluctuations in the Spatial Hydraulic Jump in Stilling Basins with Different Expansion Ratio. *Water* **2021**, *13*, 60. [CrossRef]
34. Onitsuka, K.; Akiyama, J.; Shige-Eda, M.; Ozeki, H.; Gotoh, S.; Shiraishi, T. Relationship between Pressure Fluctuations on the Bed Wall and Free Surface Fluctuations in Weak Hydraulic Jump. In *New Trends in Fluid Mechanics Research*; Springer: Berlin/Heidelberg, Germany, 2007.